STM JOURNALS

Journal of
Alternate Energy
Sources & Technologies

ISSN: 2230-7982 (Online)
ISSN: 2321-5186 (Print)
Volume 15, Issue 3, 2024
September–December
DOI (Journal): 10.37591/JoAEST

https://journals.stmjournals.com/joaest

Research JoAEST

Control System for Off-Grid Multiple Hybrid Renewables

Carlos Armenta-Déu[1,*], B. Sandoval[1]

Abstract

This article focuses on designing a renewable energy control system for a household self-consumption network, combining solar and hydroelectric energy to meet the energy demand of a standard home. We conduct an exhaustive analysis of each energy source, evaluating parameters such as solar radiation, optimal tilt of photovoltaic panels, and conversion system efficiency. Equipment for this system is selected based on the characteristics obtained in the study. Hydroelectric energy is also analyzed, considering variables such as flow rate and height of the water resource, selecting optimal equipment to maximize hydroelectric production and complement solar energy. An integrated control system is designed and implemented, efficiently managing the production and consumption of renewable energy, helping to optimize the use of energy produced, manage demand, and coordinate renewable systems. A cost-effective design is sought with a functional control system to ensure optimal management of energy resources.

Keywords: Renewable energies, solar energy, hydroelectric energy, control system, energy management, performance improvement

INTRODUCTION

Off-grid households face a fundamental challenge in obtaining a reliable energy supply to meet their daily needs. This problem is especially relevant in remote, rural areas, homes not connected to the grid, where electrical infrastructure may be limited or nonexistent. Historically, these communities have relied on traditional energy sources, such as diesel generators, with their associated costs and negative environmental impact [1–6].

However, a promising solution is emerging with the growth and advancement of renewable energy technologies. The potential to harness natural resources, such as sunlight and hydroelectric energy, offers a sustainable and economically viable alternative to supply these homes. Solar and hydroelectric energy are renewable and clean electricity generation options [7–13].

Within this frame, this work focuses on designing and developing a renewable energy control system for domestic networks under self-consumption. We propose a combination of solar and hydroelectric energy to supply the energy demand of a standard home, providing an innovative and efficient solution for those communities that lack access to the conventional electrical grid.

This work seeks to maximize the production and efficient use of the available renewable energy through an exhaustive analysis of each energy resource and the most appropriate equipment selection. Developing an integrated control system

***Author for Correspondence**
Carlos Armenta-Déu
E-mail: cardeu@fis.ucm.es

[1]Faculty, Department of Energy, Complutense University of Madrid, Madrid, Spain

Received Date: August 25, 2024
Accepted Date: August 31, 2024
Published Date: September 10, 2024

Citation: Carlos Armenta-Déu, B. Sandoval. Control System for Off-Grid Multiple Hybrid Renewables. Journal of Alternate Energy Sources & Technologies. 2024; 15(3): 20–34p.

allows optimal energy generation and consumption management, ensuring a stable and reliable supply for the proposed type of home.

FUNDAMENTALS

Solar photovoltaic power derives from solar radiation conversion into electricity through the well-known photoelectric effect [14]. The process occurs in semiconductors, which absorb solar radiation photons generating free electrons, which are removed from the semiconductor material to produce electric current [15]. The photovoltaic power generation depends on the solar radiation level and photovoltaic cell's efficiency [16]; mathematically [17]:

$$P_{PV} = \eta_{PV} G S_{PV} \tag{1}$$

P, η, and *S* are the power, efficiency, and photovoltaic panel front area and *G* is the solar radiation onto the photovoltaic panel surface. Subscript *PV* accounts for photovoltaic.

Since solar radiation evolves with daily time, modifying the photovoltaic system output power, the practical way to determine the daily energy generated by the photovoltaic system is

$$\xi_{PV} = \eta_{PV} G_{max} S_{PV} (PSH) \tag{2}$$

G_{max} corresponds to the daily solar radiation peak value, happening at solar noontime. *PSH* is the so-called "Peak Sun Hours", a measurement unit for quantifying the amount of sunlight per unit area accumulated in a specific location over a day [18]. We can reformulate Equation (2) as:

$$\xi_{PV} = \sigma_{PV} S_{PV} (PSH) \tag{3}$$

σ_{PV} is the photovoltaic panel energy density, in W/m^2, which accounts for the photovoltaic panel efficiency. Today, the most common value is around 200 W/m^2 [19].

Because of their limited output power due to the efficiency and size values, photovoltaic panels group in series and parallel tandem stack to increase voltage and current, thus power.

The outgoing energy from the photovoltaic panel suffers a reduction at the voltage converter since we have to boost the photovoltaic panel output voltage to match the local network operating one; therefore:

$$\xi_{PV} = \eta_{conv} \sigma_{PV} S_{PV} (PSH) \tag{4}$$

η_{conv} is the voltage converter efficiency.

The global photovoltaic power depends on the number of panels, N_p, in the photovoltaic set, as expressed in the following equation:

$$\xi_{PV} = N_p \eta_{conv} \sigma_{PV} S_{PV} (PSH) \tag{5}$$

Because solar radiation is intermittent and stochastic due to the day/night cycle and weather conditions [20, 21], we should include an external power source or a storage system to supply energy when solar radiation fails or is insufficient [22–24]. Hydroelectric generation is one of the most promising and environmentally friendly options among the many available solutions [25, 26]. The great advantage of hydroelectric generation is the reversible operational mode since it may operate as an energy generation device or storage system [27, 28].

Hydropower generation depends on fluid flow and hydraulic height as in [29]:

$$P_{hydro}^{t} = \eta_t \gamma \dot{V} h_t \tag{6}$$

η_t is the hydro turbine efficiency, γ is the fluid specific weight, $\dot{V}$ is the fluid volumetric flow, and h_t is the hydraulic height, which depends on the geometric height, *H*, and the mechanical losses, h_L:

$$h_t = H - h_L \tag{7}$$

Mechanical losses depend on fluid speed, *v*, duct characteristics, and geometrical shape and size [29]:

$$h_L = f\frac{L}{D_H}\frac{v^2}{2g} \tag{8}$$

Or applying the continuity equation for incompressible fluids [29]:

$$h_L = f\frac{L}{D_H^5}\frac{8\dot{V}^2}{\pi^2 g} \tag{9}$$

where *f* is the friction factor or Darcy factor, and *L* and D_H are the duct length and hydraulic diameter.

The hydraulic diameter matches the geometric one for rounded ducts; if not, we should apply the expression [29]:

$$D_H = \left(\frac{4S_{duct}}{\pi}\right)^{\frac{1}{2}} \tag{10}$$

S_{duct} represents the duct cross-section for irregular geometric shapes.

Assuming the duct is geometrically regular with a circular cross-section and combining Equations (6) to (9):

$$P_{hydro}^t = \eta_t \gamma \dot{V}\left(H - f\frac{L}{D_H^5}\frac{8\dot{V}^2}{\pi^2 g}\right) \tag{11}$$

Therefore, the generated energy by the hydropower system is:

$$\xi_{hydro}^t = \eta_t \gamma \dot{V}\left(H - f\frac{L}{D_H^5}\frac{8\dot{V}^2}{\pi^2 g}\right) t_{op}^t \tag{12}$$

t_{op}^t is the turbine daily operating time.

Reversing the operating mode of the hydraulic device and making it work as pumping system, the required power is similar to Equation (11) with the only difference of the pump efficiency, η_p:

$$P_{hydro}^p = \eta_p \gamma \dot{V}\left(H - f\frac{L}{D_H^5}\frac{8\dot{V}^2}{\pi^2 g}\right) \tag{13}$$

Superscripts *t* and *p* in Equations (11) and (13) account for turbine (power generation) and pump (hydropower storage).

Analogously, the energy consumption associated to the pumping process is:

$$\xi_{hydro}^p = \eta_p \gamma \dot{V}\left(H - f\frac{L}{D_H^5}\frac{8\dot{V}^2}{\pi^2 g}\right) t_{op}^p \tag{14}$$

t_{op}^p is the pump daily operating time.

Since power generation and energy storage do not have to match, fluid flow is different when the hydraulic system is rotating or pumping; therefore, the following equations apply:

$$\begin{aligned} P_{hydro}^t &= \eta_t \gamma \dot{V}_t\left(H - f\frac{L}{D_H^5}\frac{8\dot{V}_t^2}{\pi^2 g}\right) \\ P_{hydro}^p &= \eta_t \gamma \dot{V}_p\left(H - f\frac{L}{D_H^5}\frac{8\dot{V}_p^2}{\pi^2 g}\right) \end{aligned} \tag{15}$$

Hydropower storage consists of a natural or artificial water reservoir with a specific capacity; since natural reservoirs are not always available in the location, we propose a cylindrical tank containing the necessary water volume to generate the required power.

The water reservoir is filled and emptied at will, depending on power generation and energy storage requirements. An electronic valve controls the tank filling and emptying. The electronic valve operates based on a pressure sensor that opens or closes the valve depending on power demand or energy storage. The following equation commands the valve opening [30].

$$\left(D^{\frac{4}{3}}\frac{p_s}{\gamma}-\frac{4t\Delta P}{\pi D^{\frac{2}{3}}p_s}\right)^{\frac{3}{2}}=\frac{4\Delta P}{\pi\gamma(2g)^{\frac{1}{2}}} \tag{16}$$

where ΔP is the power differential between consumption and photovoltaic generation, p_s is the sensor pressure at the tank bottom, and t is the valve opening time.

The sensor pressure derives from the classical expression:

$$p_s=\gamma h_{tk} \tag{17}$$

where h_{tk} is the fluid height in the tank.

Replacing Equation (17) in Equation (16):

$$\left(D^{\frac{4}{3}}h_{tk}-\frac{4\gamma t\Delta P}{\pi D^{\frac{2}{3}}h_{tk}}\right)^{\frac{3}{2}}=\frac{4\Delta P}{\pi\gamma(2g)^{\frac{1}{2}}} \tag{18}$$

Since the duct diameter and water specific weight remain constant, Equation (16) converts into:

$$(\Delta P)^{\frac{2}{3}}+\Delta P\left(C_2\frac{t}{h_{tk}}\right)-C_1h_{tk}=0\ C_1=2.3\gamma^{\frac{2}{3}}D^{\frac{4}{3}};\ C_2=2.92\frac{\gamma^{\frac{5}{3}}}{D^{\frac{2}{3}}} \tag{19}$$

Equation (19) determines the valve opening time as a function of the power differential and fluid height in the tank.

PROJECT DESIGN

The project development applies to an installation 73 km from Quito (Ecuador) in a well-sunny place near a river. The building roof tilt is 25° with an azimuth of 15°. The location's geographical coordinates are provided by Google Earth application [31]. The distance from the installation to the river's closest point is less than 50 m; the available river flow, excluding ecological flow, is 1.13 m^3/s [32]. The installation is a public center operating during labor hours (8 am to 5 pm), corresponding to the highest fraction of energy consumption. Out of the labor hours, the center uses the minimum required energy to maintain the building operatives (emergency lights, standby equipment, control unit devices, alarm system, etc.).

Energy Demand

According to a previous study [33], the average monthly energy consumption is 115 to 150 kWh for the residential sector and 200 to 385 kWh for the commercial installations. Since a public building is closer to commercial energy consumption standards to ensure a sufficient power supply, we consider the maximum energy consumption rate of 385 kWh per month. Figure 1 shows the energy consumption distribution by category [34]. Table 1 shows the daily energy consumption by category for the selected installation.

We assume the monthly average energy consumption remains constant throughout the year. Since the installation only provides aggregate daily energy consumption, and because solar energy is variable throughout the day, we disaggregate daily energy consumption into hourly values applying a data

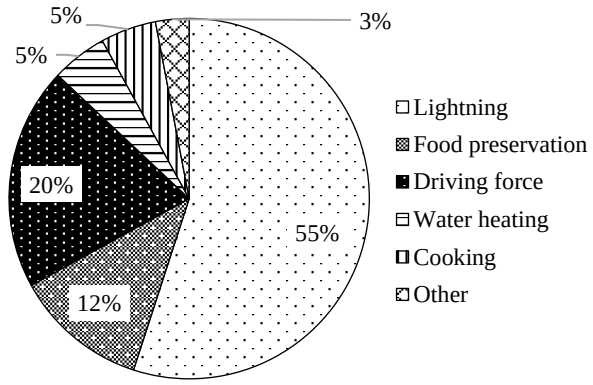

Figure 1. Energy consumption distribution [34].

Table 1. Daily and monthly average energy consumption by category [34].

Category	Daily energy consumption (kWh)	Monthly energy consumption (kWh)
Lightning	7.08	211.75
Food preservation	1.54	46.20
Driving force	2.57	77.00
Water heating	0.64	19.25
Cooking	0.64	19.25
Other	0.39	11.55
Total	*12.86*	*385.00*

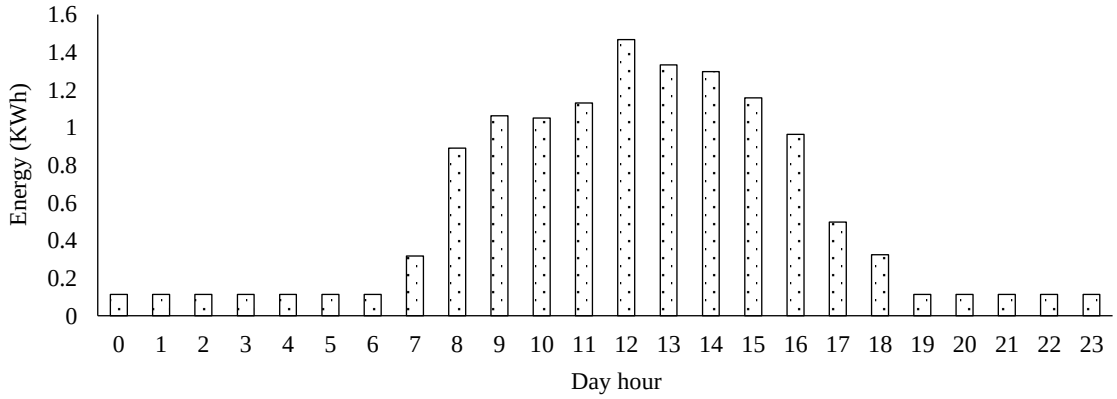

Figure 2. Hourly distribution of average daily energy consumption.

disaggregation technique specifically developed for residential, commercial and industrial energy consumption [35], obtaining (Figure 2).

SYSTEM CONFIGURATION

Photovoltaic System Selection

We selected the Qcells model Qpeak Duo of 380 Wp and 20% efficiency as the best option [36]. Figure 3 shows the photovoltaic panel technical characteristics. We have installed 10 photovoltaic panels of the mentioned model on the building rooftop preserving azimuth and tilt to avoid standing structure. The photovoltaic set is divided in two strings to avoid power supply interruption in case one of the systems fails [37]. Besides, the proposed configuration maximizes the power generation and system efficiency due to a better operation of the voltage inverter [38].

Mechanical specification

Format	1840mm × 1030mm × 32mm (including frame)
Weight	19.5kg
Front cover	2.8mm thermally pre-stressed glass with anti-reflection technology
Back cover	Composite film
Frame	Black anodised aluminium
Cell	6×22 monocrystalline Q.ANTUM solar half cells
Junction box	53-101mm × 32-60mm × 15-18mm Protection class IP67, with bypass diodes
Cable	4mm² Solar cable; (+) ≥1200mm, (-) ≥1200mm
Connector	Stäubli MC4, Hanwha Q CELLS HQC4; IP68

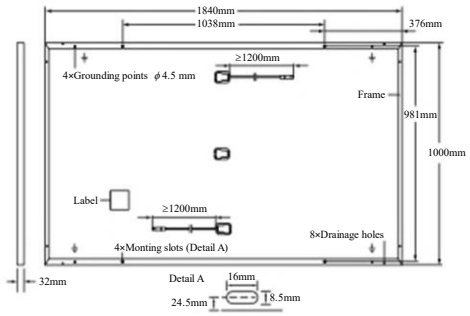

Electrical characteristics

Power class				*365*	*370*	*375*	*380*	*385*
Minimum performance at standard test conditions, STC[1] (Power tolerance +5W/-0W)								
Minimum	Power at MPP[1]	P_{MPP}	[W]	365	370	375	380	385
	Short circuit current[1]	I_{SC}	[A]	10.40	10.44	10.47	10.50	10.53
	Open circuit voltage[1]	V_{OC}	[V]	44.93	44.97	45.01	45.04	45.08
	Current at MPP	I_{MPP}	[A]	9.87	9.92	9.98	10.04	10.10
	Voltage at MPP	V_{MPP}	[V]	36.99	37.28	37.57	37.85	38.13
	Efficiency[1]	η	[%]	≥19.3	≥19.5	≥19.8	≥20.1	≥20.3
Minimum performance at normal operating conditions, NMOT[2]								
Minimum	Power at MPP	P_{MPP}	[W]	273.3	277.1	280.8	284.6	288.3
	Short circuit current	I_{SC}	[A]	8.38	8.41	8.43	8.46	8.48
	Open circuit voltage	V_{OC}	[V]	42.37	42.41	42.44	42.48	42.51
	Current at MPP	I_{MPP}	[A]	7.76	7.81	7.86	7.91	7.96
	Voltage at MPP	V_{MPP}	[V]	35.23	35.48	35.72	35.96	36.20

[1]Measurement tolerances P_{MPP} ±3%; I_{SC}; V_{OC} ±5% at STC: 1000W/m², 25±2°C, AM 1.5 according to IEC 60904-3 • [2]800W/m², NMOT, spectrum AM 1.5

Figure 3. Technical characteristics of the photovoltaic (PV) panel [38].

Solar Radiation

Photovoltaic system is powered by solar radiation; we use the PVGYS application [39] to determine the solar radiation level for specific location by simply introducing the geographical coordinates, the azimuth and the surface tilt. Since the data volume is enormous, we average hourly distribution of solar radiation to obtain the daily and monthly average solar radiation value over the year. Figure 4 shows the average hourly solar radiation evolution for the typical year.

Photovoltaic Array Engineering Design

The photovoltaic array engineering design follows the classical configuration (Figure 5). We use an 800 W inverter with double maximum power point tracking (MPPT), one for every string, operating at 115 VAC output voltage. The selected voltage corresponds to the American market, which is the operating one in Ecuador; nevertheless, the photovoltaic array configuration may operate at 220 VAC for the European market by simply changing the inverter model.

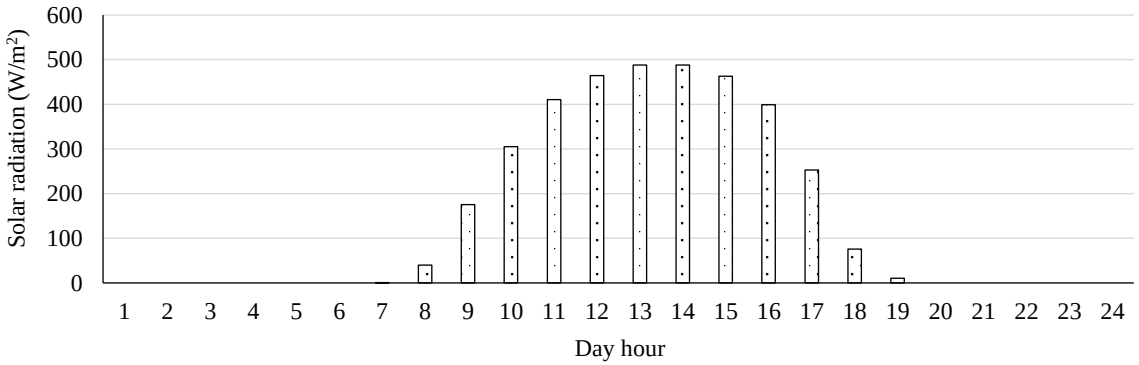

Figure 4. Average hourly distribution of solar radiation for the typical year.

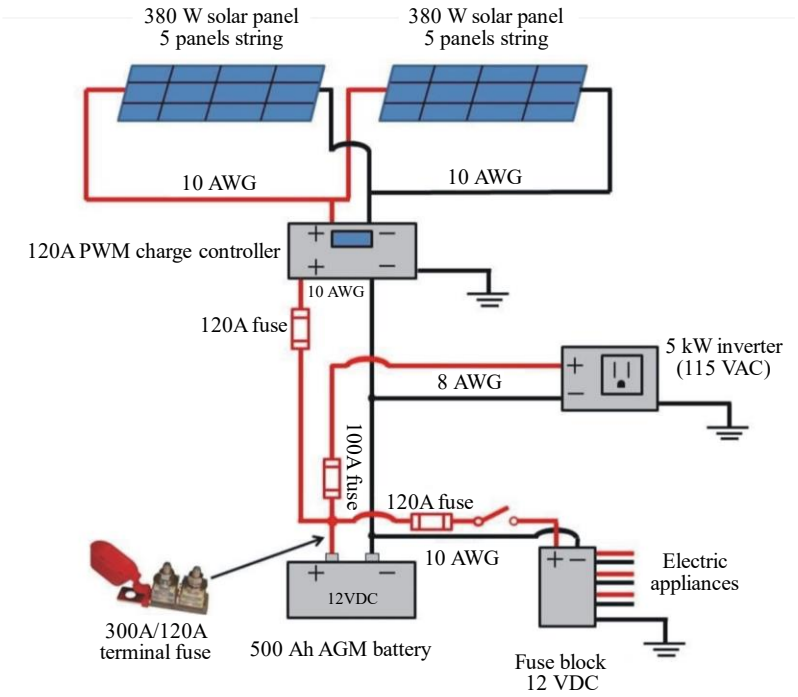

Figure 5. Layout of the photovoltaic (PV) array.

The DC junction box must have essential specific features, including the ability to couple the generator strings to the main DC cable. It must have UV protection and an IP54 protection degree. Additionally, the box should contain fuses, switches, and other electrical components. It is recommended to purchase the box according to market availability.

Because we have each string connected to an MPPT input, it is unnecessary to install fuses; however, in our case, we install fuses in all the positive and negative DC cables of the photovoltaic generator for protection. A common rule is that it must withstand at least 50% more than the short circuit current of the string. Based on this, we select a 15 A fuse.

Among the additional specifications for the inverter and the solar panel, we used a 4 mm^2 wiring thickness for the photovoltaic input and the AC output. We decided to use the H1Z2Z2-K cable from the Solflex brand, which is certified for use in photovoltaic systems and meets the necessary characteristics to ensure the safety and optimal operation of the system. For more details on its characteristics, we suggest checking the technical sheet [40].

We recommend a general switch between the box and the inverter; in some cases, technicians add a switch per panel line cable in series. This switch must withstand 1.25 I_{sc} in maximum insolation. This switch cuts off the current flow before any system overload.

Hydropower System Engineering Design

The hydropower system consists of an elevated tank, a reversible electric generator acting as a motor or generator depending on power requirements, a hsydraulic turbine, a centrifugal pump, connecting ducts, electronic valves, and a control unit. Figure 6 shows the schematic view of the system.

The hydroelectric system takes water from the river upstream of the powerhouse (water intake); water is canalized through an open canal to the water reservoir and continues canalized through a closed duct (water pipeline) until the powerhouse. The electronic valve controls the fluid flow, letting the water flow if hydropower generation is required; otherwise, it blocks the passage and stops the water flow.

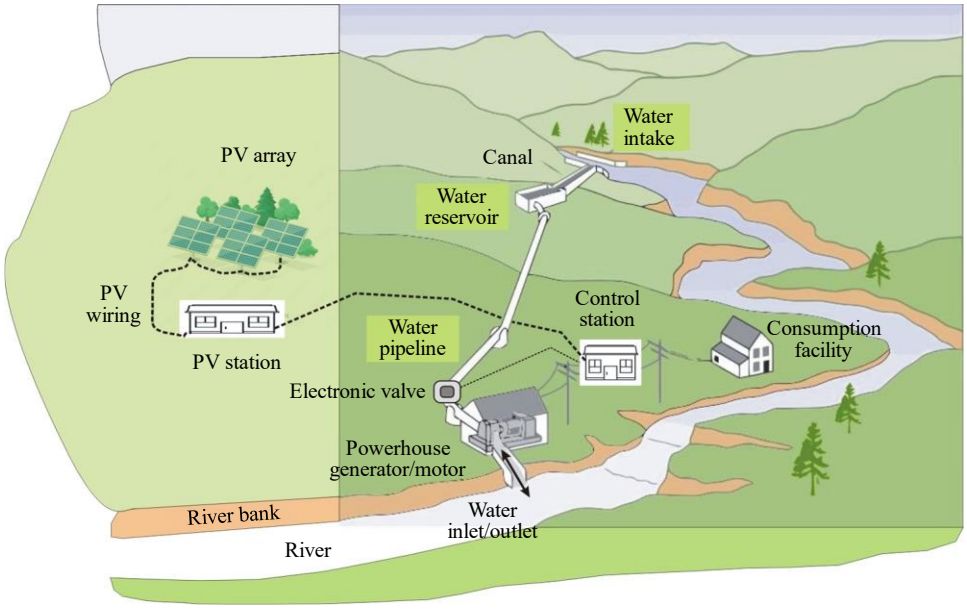

Figure 6. Hydropower system layout.

When photovoltaic generation exceeds the energy demand, the control station reverses the operating mode of the generator. It makes it work as a motor, which activates the pump located in the powerhouse and starts pumping water from the river to the water reservoir. The control station activates the electronic valve, letting the water flow through. If photovoltaic generation is insufficient to cover energy demand, the control station reverses the motor back to the generator mode, stops the pump, and activates the turbine. At this time, the electronic valve is open, and water flows from the reservoir to the powerhouse, rotating the turbine and the electric generator and producing electric energy, which supplies power to the consumption facility. The control station regulates the electronic valve opening according to the power differential between photovoltaic generation and energy demand (Equation 16). In the water pumping mode, the control station opens the electronic valve completely.

OPERATING PROTOCOL

The energy system operates under a control protocol implemented in the hardware control system located in the control station. The flowchart shown in Figure 7 describes the protocol operating mode. The control unit collects information about the photovoltaic power generation and energy demand and compares both values. If photovoltaic power generation is higher, the control unit turns the pump on and checks the water volume in the tank. If the fluid height in the tank reaches the maximum, the pump turns off, and the system commutes to the local network; otherwise, the pump turns on until the tank fills up.

On the other hand, if photovoltaic power generation equals energy demand, the control unit takes no action; for negative balance, the hydropower system turns on and checks the fluid height in the tank. If the tank is full, the control unit activates the turbine, turning it on; otherwise, the turbine switches off.

Figure 8 shows the schematic representation of the electric engineering design, with pump and turbine turned on by using a relay, depending on operating conditions. We observe that photovoltaic array connects to a shunt, which derives current to the consumption facility and pump depending on the energy balance between power generation and energy demand. The control unit regulates the current derived to the consumption facility to cover energy demand with the remaining current powering the pump unit.

The information received (electric current signal) from the pressure sensor allows the control unit to activate or deactivate the pumping system depending on the signal value. If the current corresponds to the maximum height, the relay opens, and the pump switches off because the power supply is interrupted; otherwise, the relay remains closed, and the electric current flows powering the pump.

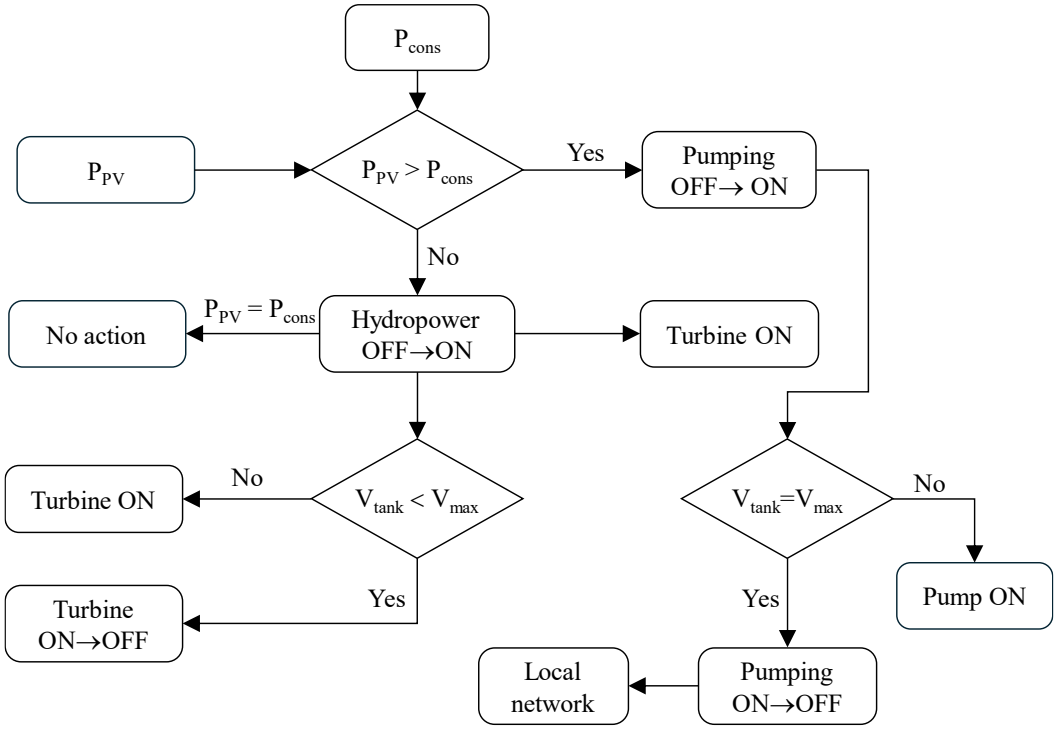

Figure 7. Operational protocol flowchart.

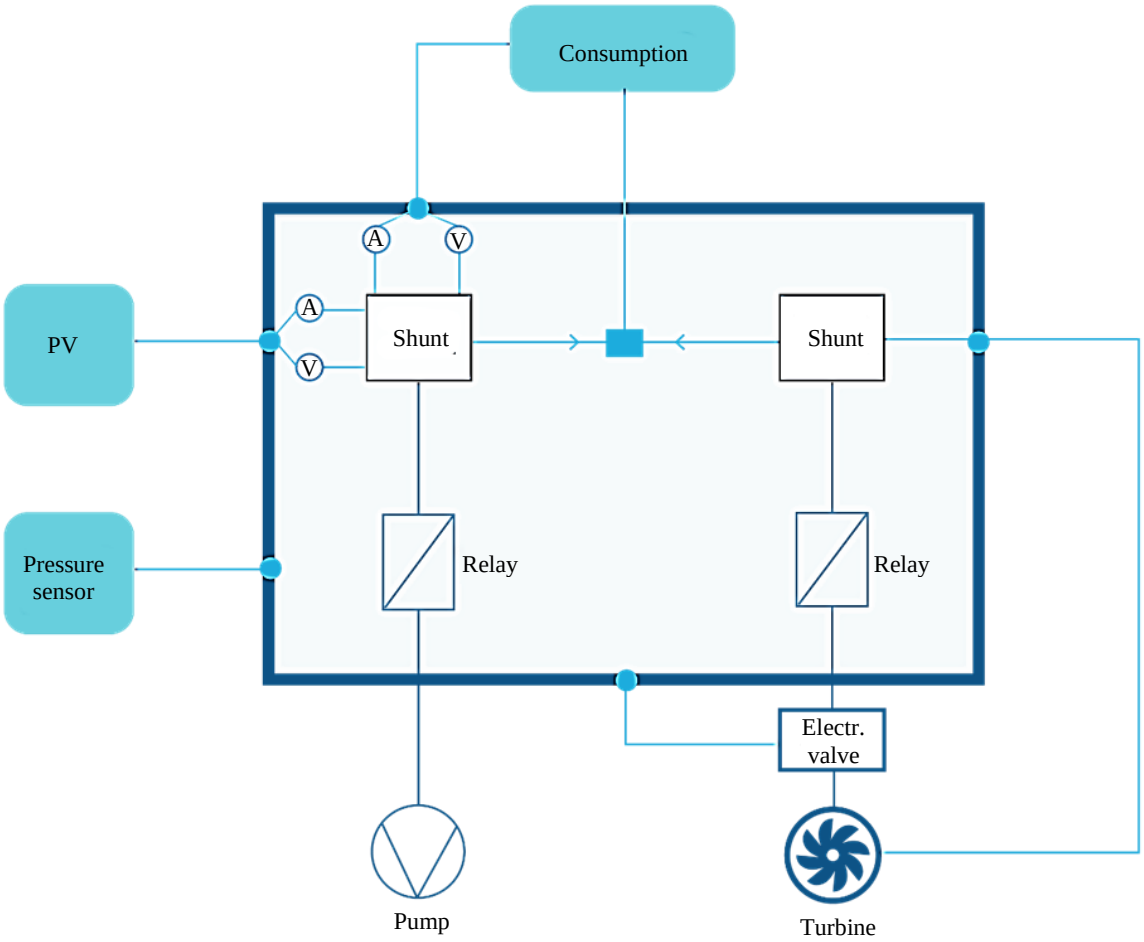

Figure 8. Schematic representation of the electric system engineering.

A second relay operates in the hydraulic turbine circuit; if the control unit detects a negative energy balance, photovoltaic power generation is lower than energy demand, the relay is closed, and the electronic valve opens, letting water flow through the turbine and supplying power to the consumption facility. The intercalated shunt in the electric turbine circuit controls the electric current supply to the electronic valve, opening the valve as necessary so that the circulating water flow results in power generation in the turbine that satisfies the condition imposed in Equation (19).

SIMULATION RESULTS

We simulate a system like the one proposed in this work to verify the validity of the engineering design and the feasibility of this project. To this goal, we apply solar radiation data and hydropower system characteristics to a prototype of a hybrid photovoltaic-hydro system with a hydraulic energy reservoir. The first simulation step consists of determining the energy balance using the following equation:

$$\Delta\xi = \xi_{PV} + \xi_{hydro} - \xi_{cons} \tag{20}$$

We calculate photovoltaic and hydroelectric energy generation, ξ_{PV}, and ξ_{hydro}, using Equations (5) and (12), respectively; the consumed energy at the consumption facility depends on the electric appliances' power and operating time. In general, we can express ξ_{cons} as:

$$\xi_{cons} = \sum_{i=1}^{n} P_i t_i \tag{21}$$

where *P* and *t* are the appliance power and operating time; subscript *i* accounts for the appliance.

Applying Equation (5) to the selected location, we obtain (Figure 9).

We observe negative values corresponding to day hours where photovoltaic arrays supply less energy than necessary to cover energy demand. In these cases, hydropower is critical to obtain a null energy balance. Considering the highest negative value for July at 8 am, we determine the tank capacity to generate enough hydroelectric power to compensate for the energy deficit.

The tank capacity depends on geometry and dimensions; in our case, we consider a cylindrical tank of specific diameter, *Dtk*, and height, *htk*. The following equation applies:

$$h_{tk} = \frac{4V_{tk}}{\pi D_{tk}^2} = \frac{4\dot{V}}{\pi D_{tk}^2} t_{op} \tag{22}$$

Now, replacing the fluid flow, $\dot{V}$, from Equation (6), we have:

$$h_{tk} = \frac{4V_{tk}}{\pi D_{tk}^2} = \frac{4}{\pi D_{tk}^2} \frac{P_{hydro}^t}{\eta_t \gamma h_t} t_{op} \tag{23}$$

Because the hydropower should match the negative energy balance:

$$h_{tk} = \frac{4}{\pi D_{tk}^2} \frac{\xi_{hydro}^t}{\eta_t \gamma h_t} = \frac{4}{\pi D_{tk}^2} \frac{(\xi_{cons} - \xi_{PV})}{\eta_t \gamma h_t} \tag{24}$$

If we express the hydraulic height, h_t, in terms of fluid flow:

$$h_t = H - f \frac{L}{D_H^5} \frac{8\dot{V}^2}{\pi^2 g} \tag{25}$$

And we replace in Equation (24), we obtain:

$$h_{tk} = \frac{4}{\pi D_{tk}^2} \frac{t_{op}}{\eta_t \gamma h_t} \left(\eta_t \gamma \dot{V} H - \eta_t \gamma f \frac{L}{D_H^5} \frac{8\dot{V}^3}{\pi^2 g} \right) \tag{26}$$

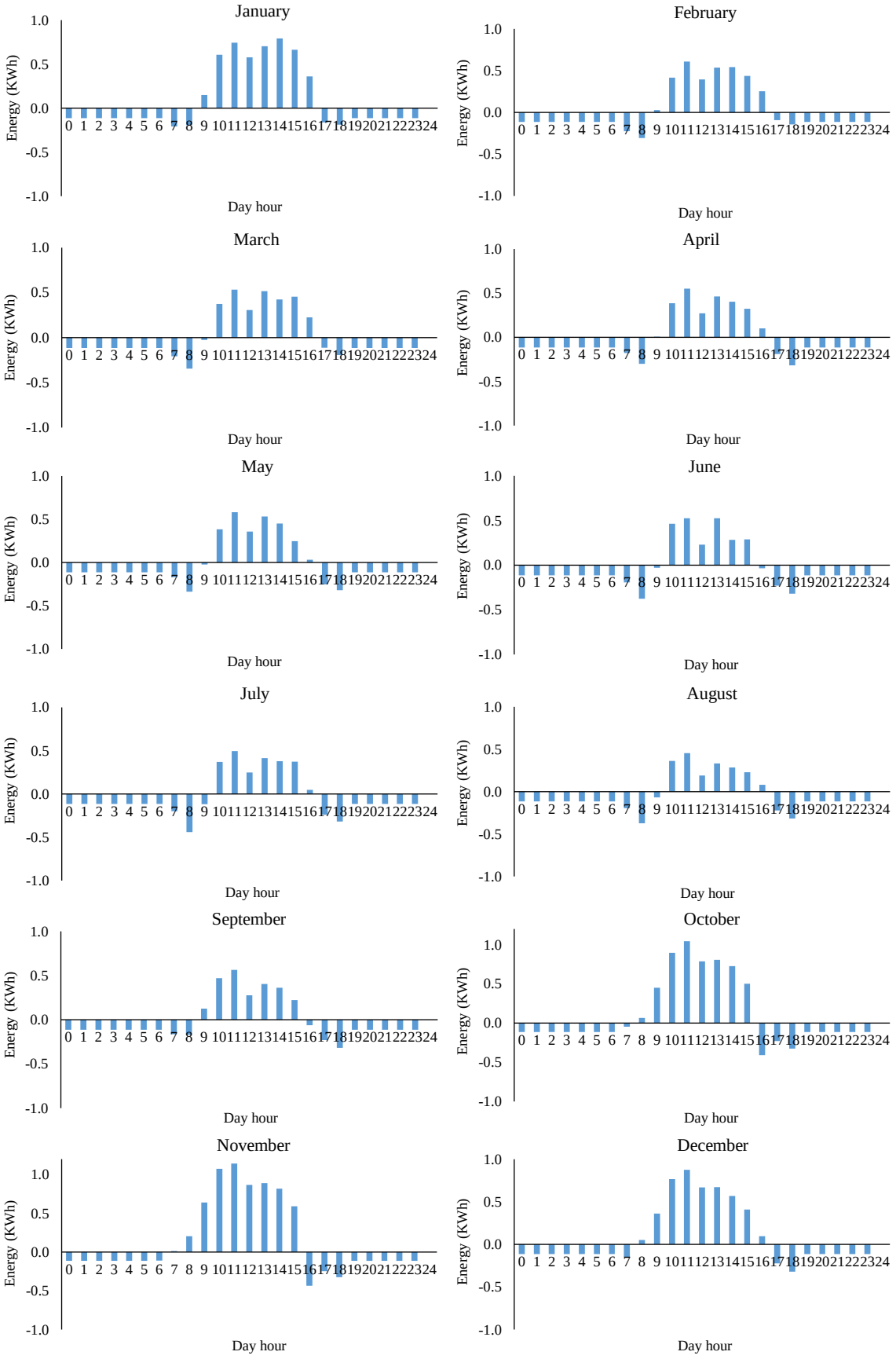

Figure 9. Monthly average hourly energy balance.

Leading to a third-degree equation of complex solution, which requires a solver program; therefore, we use the Hazen-Williams monogram [41] to obtain the hydraulic height, simplifying the solution.

Considering a tank diameter of 10 m, a turbine efficiency of 90% [42, 43], a hydraulic height of 0.65 m, and a negative energy balance of 1.62 MWh, we have:

$$h_{tk} = \frac{4}{100\pi}\frac{1.62x10^6}{(0.9)(9800)(0.65)} = 3.6\ m \tag{27}$$

We obtain the energy deficit from the value in Figure 9 for July at 8 am, which is the highest deficit in the year. Energy consumption is shown in Figure 2.

The tank height is currently oversized by 10% to avoid spillage; therefore, the effective height is 4 m. In summary, we have a tank of 10 m diameter and 4 m height, which does not represent a challenge for engineering design and manufacturing.

The inverter selection derives from the photovoltaic array operating voltage and current. Since the photovoltaic array consists of two strings of five panels each, we apply the following equations to obtain the corresponding values.

$$\begin{aligned} I_{max} &= I_{STC} + \alpha\left(T_{max}^{cell} - T_{STC}\right) \\ V_{max} &= N_p\left[V_{STC} + \beta\left(T_{min}^{cell} - T_{STC}\right)\right] \end{aligned} \tag{28}$$

The intensity value remains unchanged because the control system uses two inverters in parallel, one per string, and the panels in the string connect in series. Applying technical data from our system:

$$\begin{aligned} I_{max} &= 10.5 + 0.04(45 - 25) = 11.3\ A \\ V_{max} &= 5[37.85 - 0.27(-10 - 25)] = 236.5V \end{aligned} \tag{29}$$

Therefore, the maximum attainable power in every string is:

$$P_{max} = I_{max}V_{max} = (11.3)(236.5) = 2672.5W \tag{30}$$

Using the KACO tool [44] provided by the manufacturer, we can select the inverter compatible with the solar array. Table 2 shows the photovoltaic array and compatible inverter characteristics.

Table 2. Inverter characteristics.

System	Design result	Total	MPPT 1	MPPT 2
Photovoltaic (PV) array	Modules/string		5	5
	Number of strings		1	1
	Number of modules	10		
	STC	5880		
	PV power (Wp)	5345	2672.5	2672.5
	Min. MPP voltage (V)		228.2	228.2
	Max. V_{OC} (V)		272.45	272.45
	I_{max} (A)		11.3	11.3
	Peak voltage (V)		1000	1000
	Max. operating voltage (V)		272.45	272.45
Inverter	Efficiency	0.950		
	Min. MPP voltage (V)		112.5	112.5
	Max. operating voltage (V)		580	580
	Max. input current (A)		12.0	12.0

An alternative to the selected photovoltaic array and inverter system is using photovoltaic panels equipped with micro-inverters. This configuration reduces significantly the power losses; indeed, the calculation of power losses for every case produces the following results:

$$P_L^{conv} = I^2R = (11.3)^2(0.051) = 6.5W$$
$$P_L^{micro} = \left(\frac{I}{N_p}\right)^2 R = \left(\frac{11.3}{5}\right)^2 (0.051) = 0.26W \quad (31)$$

We notice the power losses using a conventional configuration are 25 times higher. Power losses represent 0.3% and 0.008% of the global power generation for every case, conventional a micro-inverter configuration. Panels with micro-inverters stand out for their greater efficiency since they operate independently, mitigating partial shading problems or failures in an individual panel. However, its 2.5 times higher initial cost and system complexity can make installation and maintenance difficult [45].

On the other hand, conventional solar panels with an independent inverter have a lower initial cost and easy installation due to the smaller number of components. However, they show efficiency problems because the shading or failures in one panel affect the entire system. However, today, most solar panels build bypass diodes that allow the electric current to bypass the shaded cells, avoiding energy loss and overheating. Having mentioned the peculiarities of both panels, we decided that the losses using conventional panels for our system are low; therefore, we selected the classical configuration.

CONCLUSIONS

In this work, we have designed and developed a renewable energy control system for a self-consumption facility, combining solar and hydroelectric energy through a detailed analysis of the available energy resources and selecting the most appropriate equipment. The integrated control system developed in this work allows for optimal energy generation and consumption management, maximizing production and efficient use of available renewable sources. The implementation of this system ensures a stable and reliable energy supply for the proposed type of home.

In conclusion, this work has demonstrated the technical feasibility of combining solar and hydroelectric energy for self-consumption, laying the foundations for future research and development in more detail of our sizing.

REFERENCES

1. Lacayo AI. Off-grid energy in rural India: policy recommendations for effective UN projects. WWS Undergraduate Task Force: Energy for Sustainable Development; 2006.
2. Cook P. Infrastructure, rural electrification and development. Energy Sustain Dev. 2011; 15 (3): 304–313.
3. Zomers A. Remote access: context, challenges, and obstacles in rural electrification. IEEE Power Energy Mag. 2014; 12 (4): 26–34.
4. Samanta KP. A study of rural electrification infrastructure in India. J Business Manage. 2015; 17: 54–59.
5. Barnes DF. The challenge of rural electrification. In: The Challenge of Rural Electrification: Strategies for Developing Countries. New York, NY, USA: Routledge; 2010. pp. 1–17.
6. Johnson NG, Bryden KM. Energy supply and use in a rural West African village. Energy. 2012; 43 (1): 283–292.
7. Arungu-Olende S. Rural energy. Nat Resour Forum. 1984; 8 (2): 117–126.
8. Neto MB, Carvalho PCM, Carioca JOB, Canafístula FJF. Biogas/photovoltaic hybrid power system for decentralized energy supply of rural areas. Energy Policy. 2010; 38 (8): 4497–4506.
9. Bronicki LY. Sustainable energy for rural areas of the developing countries. Energy Environ. 2002; 13 (4–5): 515–522.

10. Woldeyohannes AD, Woldemichael DE, Baheta AT. Sustainable renewable energy resources utilization in rural areas. Renew Sustain Energy Rev. 2016; 66: 1–9.
11. Cherni JA, Dyner I, Henao F, Jaramillo P, Smith R, Font RO. Energy supply for sustainable rural livelihoods. A multi-criteria decision-support system. Energy Policy. 2007; 35 (3): 1493–1504.
12. de Almeida A, Moura P, Quaresma N. Energy-efficient off-grid systems. Energy Efficiency. 2020; 13 (2): 349–376.
13. Benedek J, Sebestyén TT, Bartók B. Evaluation of renewable energy sources in peripheral areas and renewable energy-based rural development. Renew Sustain Energy Rev. 2018; 90: 516–535.
14. Klassen S. The photoelectric effect: reconstructing the story for the physics classroom. Sci Educ. 2011; 20: 719–731.
15. Luque A, Hegedus S, editors. Handbook of Photovoltaic Science and Engineering. Hoboken, NJ, USA: John Wiley & Sons; 2011.
16. McEvoy A, Markvart T, Castañer L, Markvart T, Castaner L, editors. Practical Handbook of Photovoltaics: Fundamentals and Applications. New York, NY, USA: Elsevier; 2003.
17. Kalogirou S, editor. McEvoy's Handbook of Photovoltaics: Fundamentals and Applications. San Diego, CA, USA: Academic Press.
18. El Idrissi YA. Peak Sun Hours Calculator, Definition, Maps, and Data. [Online]. Renewable Wise. March 16, 2024. Available at https://www.renewablewise.com/peak-sun-hours-calculator/.
19. Markvart T, Castañer L, editors. Practical Handbook of Photovoltaics: Fundamentals and Applications. New York, NY, USA: Elsevier; 2003.
20. Farahmand MZ, Nazari ME, Shamlou S, Shafie-Khah M. The simultaneous impacts of seasonal weather and solar conditions on PV panels electrical characteristics. Energies. 2021; 14 (4): 845.
21. Shadid R, Khawaja Y, Bani-Abdullah A, Akho-Zahieh M, Allahham A. Investigation of weather conditions on the output power of various photovoltaic systems. Renew Energy. 2023; 217: 119202.
22. Kosonen I. Intermittency of Renewable Energy; Review of Current Solutions and Their Sufficiency. Bachelor's Thesis. Lappeenranta, Finland: Lappeenranta University of Technology; 2018.
23. Wu C, Zhang XP, Sterling M. Solar power generation intermittency and aggregation. Sci Rep. 2022; 12 (1): 1363.
24. Sorensen B. Energy Intermittency. Boca Raton, FL, USA: CRC Press; 2018.
25. Chang MK, Eichman JD, Mueller F, Samuelsen S. Buffering intermittent renewable power with hydroelectric generation: a case study in California. Appl Energy. 2013; 112: 1–11.
26. Kaygusuz K. Hydropower as clean and renewable energy source for electricity generation. J Eng Res Appl Sci. 2016; 5 (1): 359–369.
27. Rehman S, Al-Hadhrami LM, Alam MM. Pumped hydro energy storage system: a technological review. Renew Sustain Energy Rev. 2015; 44: 586–598.
28. Jurasz J, Mikulik J, Krzywda M, Ciapała B, Janowski M. Integrating a wind- and solar-powered hybrid to the power system by coupling it with a hydroelectric power station with pumping installation. Energy. 2018; 144: 549–563.
29. Cengel Y, Cimbala J. Fluid Mechanics Fundamentals and Applications (SI Units). New York, NY, USA: McGraw Hill; 2013. Ebook.
30. Sandoval NB. Control System for Off-grid Multiple Hybrid Renewable Energy Source. Master's Thesis. Madrid, Spain: Complutense University of Madrid; 2024.
31. Google Earth. El globo terráqueo más complete. [Online]. Available at https://www.google.es/intl/es/earth/index.html
32. Empresa pública metropolitana de agua potable y saneamiento EPMAPS. Resumen ejecutivo de estudio de impacto ambiental y plan de manejo ambiental, Capitulo 3.1.4 Hidrología.
33. Escuela Politécnica Nacional. Análisis de los consumos energéticos en Ecuador, Capitulo 2. 2018.
34. CONELEC. Análisis previo para realizar una investigación sobre los usos finales de energía en los sectores residencial, comercial e industrial, año 2008.
35. Armenta-Déu C. Disaggregation of Average Daily Data into Hourly Values for Residential, Commercial and Industrial Energy Consumption Facilities. Project RUTW-13/06. Internal Report GER 14/01 (Restricted). 2014.

36. Qcells. PV solar panel Q.peak Duo BLK ML-G9 Series 375-395 Wp. [Online]. Available at https://es.enfsolar.com/pv/panel-datasheet/crystalline/54343.
37. Walker GR, Xue J, Sernia P. PV string per-module maximum power point enabling converters. In: Australasian Universities Power Engineering Conference, AUPEC'03, Christchurch, New Zealand, January 1, 2003.
38. Qcells. Solar panel technical datasheet. Q.peak Duo BLK ML-G9 Series 375-395 Wp. [Online]. Available at https://cdn.enfsolar.com/z/pp/85n4ncmjh/Q-CELLS-Data-sheet-Q.PEAK-DUO-BLK-ML-G9-QD-365-385-2021-01-R.pdf
39. European Commission. Photovoltaic geographical information system (PVGIS). [Online]. Available at https://re.jrc.ec.europa.eu/pvg_tools/es/
40. Migueles F. Solflex cable technical datasheet H1Z2Z2K. [Online]. 2024. Available at https://www.miguelez.com/descargas/productos/H1Z2Z2-K%20ES%20wI.pdf
41. Kundu PK, Cohen IM, Dowling DR. Fluid Mechanics. San Diego, CA: Academic Press; 2015.
42. Liu X, Luo Y, Karney BW, Wang W. A selected literature review of efficiency improvements in hydraulic turbines. Renew Sustain Energy Rev. 2015; 51: 18–28.
43. Gordon JL. Hydraulic turbine efficiency. Can J Civil Eng. 2001; 28 (2): 238–253.
44. Kaco. String sizing tool. [Online]. Available at https://kaco-newenergy.com/string-sizing-tool
45. Sunfields Europe. Placas solares con microinversores. [Online]. Available at https://www.sfe-solar.com/instalaciones-fotovoltaicas/productos/paneles-solares/inversor-integrado/

